Hard-surface effects in polymer self-consistent field calculations

Dong Meng and Qiang Wang[a)]
Department of Chemical and Biological Engineering, Colorado State University, Fort Collins, Colorado 80523-1370

(Received 26 February 2007; accepted 23 April 2007; published online 19 June 2007)

We have investigated several effects due to the confinement of polymer melts by impenetrable (hard) surfaces in the self-consistent field calculations. To adequately represent such confinement, the total (normalized) polymer segmental density (volume fraction) is usually constrained to an imposed profile that continuously decreases from 1 in the interior of confined melts to 0 at the surfaces over a short distance. The choice of this profile strongly influences the numerical performance of the self-consistent field calculations. In addition, for diblock copolymers *A-B* the hard-surface confinement has both energetic and entropic effects: On one hand, the decrease of polymer density from 1 reduces *A-B* repulsion and favors morphologies with more *A-B* interfaces near the surfaces. On the other hand, the enrichment of chain ends and depletion of middle segments near the surfaces favor parallel morphologies where chains orient mainly perpendicular to the surfaces. These two effects are comparable in magnitude, and for asymmetric diblock copolymers result in an entropic preference of a neutral surface for the shorter block as proposed previously [Q. Wang *et al.*, Macromolecules **34**, 3458 (2001)]. The hard-surface effects are weak in practice and thus manifested only when the surfaces are nearly neutral. © *2007 American Institute of Physics*. [DOI: 10.1063/1.2740633]

I. INTRODUCTION

Proposed over 40 years ago,[1] the self-consistent field (SCF) theory has been widely applied to various polymeric systems with great success, including the interface of polymer blends,[2–9] microphase separation of block copolymers,[10–12] polymers near surfaces,[13,14] etc. Advanced numerical methods[15–18] and parallelization[19] enable SCF calculations with high accuracy, providing a mature and powerful computational tool for the study of equilibrium behavior of polymeric systems at nanoscale to mesoscale.

In the most common form of SCF theory for polymer melts, the incompressibility constraint is enforced, which requires the total (normalized) polymer segmental density (volume fraction) being 1 everywhere in the system.[20] When applied to polymer melts confined by impenetrable (hard) surfaces, however, such SCF calculations encounter some numerical problems that have not been examined closely. To adequately represent the hard-surface confinement, the polymer density right at the surface must vanish, requiring the end-integrated propagator $q(\mathbf{r},s)$ be 0 there for all s (a variable denoting the segmental position along the chain contour). According to the modified diffusion equation $\partial q/\partial s = \nabla^2 q - \omega(\mathbf{r})q$, this leads to a diverging conjugate field $\omega(\mathbf{r})$ unless $\nabla^2 q$ is 0 for all s at the surface. Such a diverging ω field may cause some numerical problems, not only in solving the SCF equations, but also in calculating the system free energy.

On the other hand, the vanishing polymer density at the surface is incompatible with the incompressibility constraint. A common way to circumvent this is to replace 1 in the incompressibility constraint by a function $\phi_0(\mathbf{r})$ that continuously varies from 0 to 1 over a short distance from the surface (surface layer). The choice of $\phi_0(\mathbf{r})$ in the surface layer, however, has been arbitrary. While Matsen used a cosine-shape profile,[21] Chen and Fredrickson adopted a linear profile;[22] Li *et al.* used a "step-function" profile,[23] which can be considered as a linear profile due to the spatial domain discretization. Because of the continuous Gaussian chain model commonly used in SCF theory, it cannot capture the polymer density oscillations near an impenetrable surface (which is due to the chain packing effects) as revealed, for example, by Monte Carlo simulations.[24] The choice of $\phi_0(\mathbf{r})$ should therefore be based on the numerical performance of SCF calculations, i.e., to make the calculations converge rapidly with refined discretization. Although it has been claimed that the detailed shape of $\phi_0(\mathbf{r})$ in the surface layer has little consequence, our results show that this is not the case in terms of the numerical performance of SCF calculations, as demonstrated with a model system of confined homopolymer melts in Sec. III.

In addition to the above numerical problems, hard-surface confinement as modeled in SCF calculations influences the system in two different but related aspects: the decrease of polymer density near the surface and the change of chain conformations from the bulk counterparts [where $\phi_0(\mathbf{r})=1$]; the latter is manifested by chain-end enrichment and middle-segment depletion near the surface. For the self-assembly of block copolymers under nanoconfinement, which has attracted great interest in recent years due to its potential applications in nanotechnology,[25–27] these correspond to energetic and entropic effects, respectively. The former has been referred to as the "surface-induced compatibilization" between different types of polymer segments, and

[a)]Electronic mail: q.wang@colostate.edu

considered as the dominant factor responsible for the interesting phenomenon that, when the film thickness is commensurate with the bulk lamellar period, perpendicular lamellae are more stable than parallel lamellae in thin films of symmetric diblock copolymers confined between two neutral surfaces.[21,24,28] Our results in Sec. IV show, however, that the entropic effects are comparable in magnitude to this energetic effect and cannot be overlooked. In fact, Monte Carlo simulations have revealed that chain ends enrich near a hard surface and that diblock copolymer chains close to the surface orient parallel to it.[29,30] In the case of asymmetric diblock copolymer thin films, one of us further proposed that a neutral surface exhibits an entropic preference for the shorter block due to chain-end enrichment.[31]

From theoretical point of view, it is of fundamental interest in polymer science to understand how an impenetrable surface affects the behavior of polymers near it. In this work, we present a systematic study on the hard-surface effects in SCF calculations. Our models and numerical methods are summarized in Sec. II. In Sec. III we identify two profiles of $\phi_0(\mathbf{r})$ in the surface layer that are suitable for high-accuracy SCF calculations of confined polymer melts. We then in Sec. IV investigate both the energetic and entropic effects of hard-surface confinement on symmetric diblock copolymer thin films. These effects for cylinder-forming asymmetric diblock copolymer thin films are further examined in Sec. V. Section VI is devoted to conclusions.

II. MODELS AND NUMERICAL METHODS

Since the polymer SCF theory has been well developed, we only summarize our SCF equations and numerical methods here; readers are referred to, e.g., Ref. 32 for detailed derivation and explanation of this theory.

A. Confined homopolymer melts

The simplest case is to confine homopolymers A with a length N_A to a one-dimensional polymer segmental density (normalized by the bulk density of polymer segments) profile $\phi_0(x)$, where $x\in[0,d]$ and $\phi_0(x=0)=\phi_0(x=d)=0$. The corresponding SCF equations are

$$\frac{\partial q}{\partial s}=\frac{\partial^2 q}{\partial x^2}-\eta(x)q, \tag{1}$$

$$\phi_0(x)=\frac{\bar{\phi}_0 N}{QN_A}\int_0^{N_A/N}\mathrm{d}s q(x,s)q\left(x,\frac{N_A}{N}-s\right). \tag{2}$$

Here $q(x,s)$ corresponds to the probability of finding the end segment of a polymer chain of length sN at x, and $s\in[0,N_A/N]$ denotes a position along the chain contour. $\eta(x)$ is the (purely imaginary) pressure field enforcing the confinement, Eq. (2); note that $\eta(x)$ can be shifted by an arbitrary constant. The boundary conditions for the modified diffusion equation, Eq. (1), are $q(x=0,s)=q(x=d,s)=0$ for all s, and its initial condition is $q(x,s=0)=1$ for $0<x<d$. In Eq. (2), $\bar{\phi}_0\equiv\int_0^d\mathrm{d}x\phi_0(x)/d$, and the single-chain partition function $Q\equiv\int_0^d\mathrm{d}xq(x,N_A/N)/d$. Note that x is in units of the radius of gyration of a Gaussian chain of N segments, $R_g\equiv a\sqrt{N/6}$, where a denotes the statistical segment length; for finite N_A, we set $N=N_A$ hereafter. Once the SCF equations are solved, the mean-field free energy per polymer segment is given by

$$F_s=-\frac{1}{N}\left[\frac{1}{\bar{\phi}_0 d}\int_0^d\mathrm{d}x\eta(x)\phi_0(x)+\ln\bar{\phi}_0\right], \tag{3}$$

where we have set $Q=\bar{\phi}_0$ to obtain a unique solution of $\eta(x)$.

To solve $\eta(x)$ for a given $\phi_0(x)$, we invoke the ground-state dominance approximation (GSDA), which gives $q(x,s)=\exp(-\eta_0 s)q_0(x)$ for $N_A\to\infty$, where η_0 is the smallest eigenvalue of the operator $-\partial^2/\partial x^2+\eta(x)$, and $q_0(x)$ is the corresponding eigenfunction. Substituting it into the SCF equations, we obtain

$$\eta^{\mathrm{GSDA}}(x)=\frac{\phi_0''}{2\phi_0(x)}-\left[\frac{\phi_0'}{2\phi_0(x)}\right]^2, \tag{4}$$

where ϕ_0' denotes $\mathrm{d}\phi_0(x)/\mathrm{d}x$, and so on. Note that a constant is ignored in Eq. (4). As shown below, this relation can help us understand the behavior of $\eta(x)$ obtained by numerically solving the SCF equations.

To ensure the high accuracy of our numerical results, we use the newly proposed fourth-order implicit-explicit scheme[17] to solve the modified diffusion equation. The chain contour $[0,1]$ is uniformly discretized into n steps. To obtain the initial values for q required by this method, we use the second-order pseudospectral method[16] (instead of the first-order Euler method as proposed in Ref. 17) combined with Richardson extrapolation.[33] In the x direction, we use fast sine transforms, consistent with the boundary conditions of the modified diffusion equation. The SCF equations are solved in real space by the Broyden method combined with a globally convergent strategy.[34] The interval $[0,d]$ is uniformly discretized into m subintervals, and the absolute residual error of Eq. (2) at any collocation point is less than 10^{-10} in our calculations. Finally, we evaluate all integrals using Romberg integration.[35]

B. Confined diblock copolymer melts

Here we consider diblock copolymers A-B of chain length N confined between two flat and impenetrable surfaces placed at $x=0$ and d. Assuming that all polymer segments have the same statistical segment length a, we can write the SCF equations as

$$\omega_A(\mathbf{r})=\chi N\phi_B(\mathbf{r})-H(x)+\eta(\mathbf{r}), \tag{5}$$

$$\omega_B(\mathbf{r})=\chi N\phi_A(\mathbf{r})+H(x)+\eta(\mathbf{r}), \tag{6}$$

$$\phi_A(\mathbf{r})=\frac{\bar{\phi}_0}{Q}\int_0^{f_A}\mathrm{d}s q(\mathbf{r},s)q^*(\mathbf{r},1-s), \tag{7}$$

$$\phi_B(\mathbf{r})=\frac{\bar{\phi}_0}{Q}\int_{f_A}^{1}\mathrm{d}s q(\mathbf{r},s)q^*(\mathbf{r},1-s), \tag{8}$$

$$\phi_A(\mathbf{r}) + \phi_B(\mathbf{r}) = \phi_0(x). \tag{9}$$

Here $\phi_A(\mathbf{r})$ and $\phi_B(\mathbf{r})$ are the density fields of A and B segments, respectively, and $\omega_A(\mathbf{r})$ and $\omega_B(\mathbf{r})$ are the (purely imaginary) conjugate fields interacting with these species. $\eta(\mathbf{r})$ enforces the incompressibility, Eq. (9) in this case. $H(x)$ is a field representing the energetic surface preference for the two blocks: it is positive when the surface prefers A segments and negative when the surface prefers B segments; in most cases we use two neutral surfaces and set $H(x)=0$. We also use χ to denote the Flory-Huggins interaction parameter between A and B segments, f_A the volume fraction of A block in the copolymer, and $s \in [0,1]$ the segmental position along the chain contour.

For diblock copolymers, $q(\mathbf{r},s)$ corresponds to the probability of finding a copolymer chain of length sN that starts from the A end (where $s=0$) anywhere in the system and ends at position $\mathbf{r}$, and satisfies

$$\frac{\partial q}{\partial s} = \begin{cases} \nabla^2 q - \omega_A(\mathbf{r}) q & \text{for } 0 \leqslant s \leqslant f_A \\ \nabla^2 q - \omega_B(\mathbf{r}) q & \text{for } f_A \leqslant s \leqslant 1. \end{cases} \tag{10}$$

Similarly, $q^*(\mathbf{r},t)$ with $t \equiv 1-s$ corresponds to the probability of finding a copolymer chain of length tN that starts from the B end (where $s=1$) anywhere in the system and ends at $\mathbf{r}$, and satisfies

$$\frac{\partial q^*}{\partial t} = \begin{cases} \nabla^2 q^* - \omega_B(\mathbf{r}) q^* & \text{for } 0 \leqslant t \leqslant 1 - f_A \\ \nabla^2 q^* - \omega_A(\mathbf{r}) q^* & \text{for } 1 - f_A \leqslant t \leqslant 1. \end{cases} \tag{11}$$

Two sets of boundary and initial conditions for the modified diffusion equations, Eqs. (10) and (11), are used in our calculations. For cases where $\phi_0(x=0)=\phi_0(x=d)=0$, unless otherwise specified, we apply the Dirichlet boundary conditions of $q(\mathbf{r},s)=q^*(\mathbf{r},s)=0$ at $x=0$ and d for all s, together with the initial conditions of $q(\mathbf{r},s=0)=q^*(\mathbf{r},t=0)=1$ at $0<x<d$; while for all other cases, we apply the Neumann boundary conditions of $\partial q(\mathbf{r},s)/\partial x = \partial q^*(\mathbf{r},s)/\partial x = 0$ at $x=0$ and d for all s, together with the initial conditions of $q(\mathbf{r},s=0)=q^*(\mathbf{r},t=0)=1$ at all $\mathbf{r}$. For multidimensional calculations, periodic boundary conditions are applied in the y and z directions. In Eqs. (7) and (8), $Q \equiv \int d\mathbf{r} q(\mathbf{r},1)/V$ and $\bar{\phi}_0 \equiv \int_0^d dx \phi_0(x)/d$, where $V=l_y l_z d$ denotes the system volume with l_y and l_z being the system sizes along the y and z directions, respectively. Again, we have normalized all the distance by $R_g \equiv a\sqrt{N/6}$. Once the SCF equations are solved, the mean-field free energy per chain of length N is calculated as

$$F = \frac{1}{\bar{\phi}_0 V} \int d\mathbf{r} \{\chi N \phi_A(\mathbf{r}) \phi_B(\mathbf{r}) - \omega_A(\mathbf{r}) \phi_A(\mathbf{r}) - \omega_B(\mathbf{r}) \phi_B(\mathbf{r}) - H(x)[\phi_A(\mathbf{r}) - \phi_B(\mathbf{r})]\} - \ln Q. \tag{12}$$

As before, we use the fourth-order implicit-explicit scheme[17] to solve the modified diffusion equations. The chain contour $[0,1]$ is uniformly discretized into n steps, and the interval $[0,d]$ (in the x direction) is uniformly discretized into m subintervals. We use the fast sine transforms in the x direction when the Dirichlet boundary conditions are applied, and the fast cosine transforms when the Neumann boundary conditions are applied. For multidimensional calculations, the system sizes along the y and z directions are uniformly discretized into m_y and m_z subintervals, respectively, and we use the fast Fourier transforms in these directions. For one-dimensional calculations, the Broyden method is used to solve the SCF equations and the maximum residual error at all collocation points $\mathbf{r}$, $\epsilon \equiv \max\{|(\omega_A(\mathbf{r}) - \omega_B(\mathbf{r}))/2\chi N + \phi_0(x)/2 - \phi_B(\mathbf{r})|, |(\omega_B(\mathbf{r}) - \omega_A(\mathbf{r}))/2\chi N + \phi_0(x)/2 - \phi_A(\mathbf{r})|\}$, is less than 10^{-11}; while for multidimensional calculations, the semi-implicit scheme[18] is used to iterate the SCF equations till ϵ is less than 10^{-4}; here, for given $\omega_A(\mathbf{r})$ and $\omega_B(\mathbf{r})$, Eqs. (7) and (8) are used to calculate $\phi_A(\mathbf{r})$ and $\phi_B(\mathbf{r})$ after the modified diffusion equations are solved. Since the conjugate fields can be shifted by an arbitrary constant without changing the density fields and the system free energy, we set $Q=\bar{\phi}_0/3n$ to obtain a unique solution. Finally, we evaluate all integrals using Romberg integration[35] when possible; the composite Simpson's formula is used otherwise.

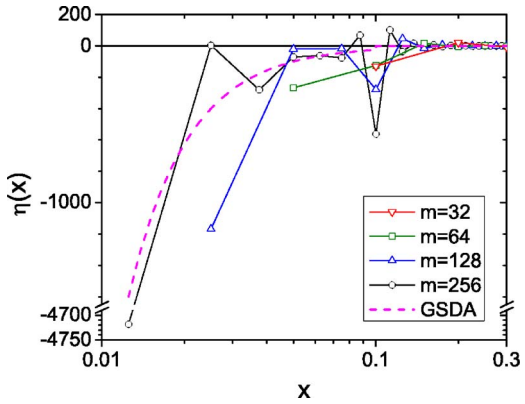

FIG. 1. Pressure field $\eta(x)$ for confined homopolymer melts, with the linear profile P1 used in the surface layer. $d=3.2$, $\tau=0.1$, and $n=2048$.

III. CONFINED HOMOPOLYMERS

A. Choice of $\phi_0(x)$

In the interior of confined polymer melts it is natural to set the (normalized) polymer segmental density $\phi_0(x)=1$, while close to the confining surfaces $\phi_0(x)$ continuously decreases from 1 to 0 over a short distance denoted by τ (surface layer). Thus our goal here is to identify a form of $\phi_0(x)$ in the surface layer, denoted by $\phi_{0,\mathrm{sl}}(x)$ with $x \in [0,\tau]$ that leads to good numerical performance of SCF calculations (i.e., makes the calculations converge rapidly with increasing m and n); for this purpose, we consider $\phi_0(x)$ to be symmetric about $x=d/2$.

Most SCF calculations in the literature used a linear profile of $\phi_{0,\mathrm{sl}}(x)=x/\tau$ (referred to as P1); this includes the "step-function" case [i.e., $\phi_{0,\mathrm{sl}}(x=0)=0$ and $\phi_{0,\mathrm{sl}}(x>0)=1$][23,36] due to the discretization in the x direction. Figure 1 shows the obtained pressure field $\eta(x)$ for this P1 profile, where $d=3.2$ and $\tau=0.1$ are used with different values of m. Our calculation with $m=32$ corresponds to the "step-function" case, while that with $m=64$ corresponds to the profile used in Refs. 22, 37, and 38. Although these two

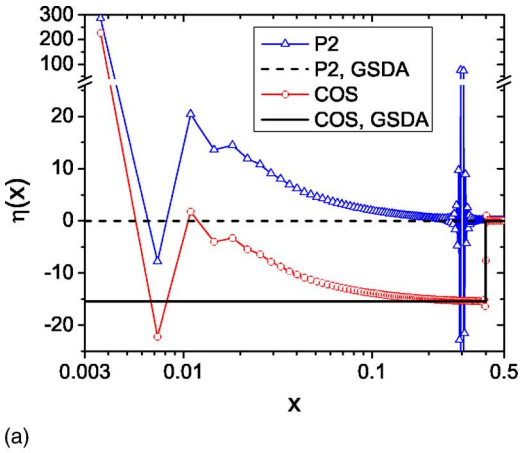

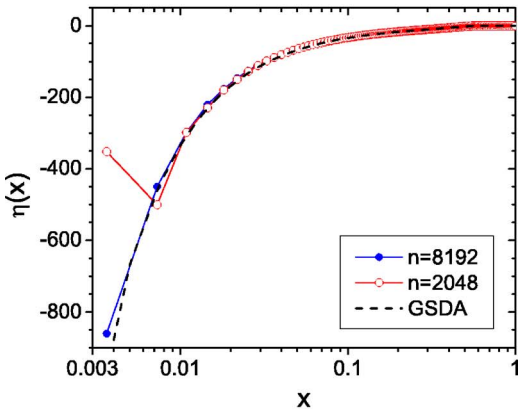

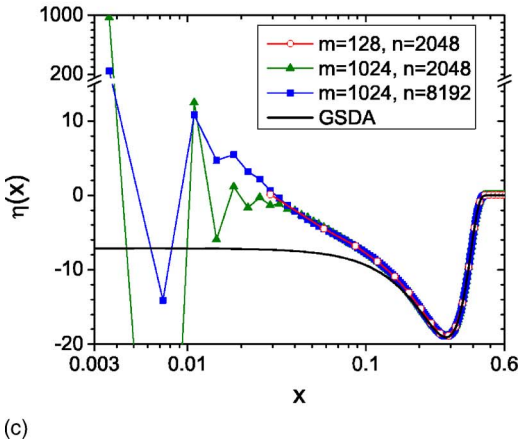

FIG. 2. Pressure field $\eta(x)$ for confined homopolymer melts, where $d \approx 3.7237$ and the τ values are chosen to give the same $\bar{\phi}_0$ in all cases: (a) The quadratic profile P2 ($\tau=0.3$) and the cosine profile COS ($\tau=0.4$) are used in the surface layer, respectively. $m=1024$ and $n=2048$. In the P2 case, two data points located around $x=\tau$ with η values less than -500 are not shown. (b) The fifth-order polynomial P5 ($\tau=0.6$) is used in the surface layer. $m=1024$. (c) The profile EXP ($\tau \approx 0.5303$) is used in the surface layer. For the case of $m=1024$ and $n=2048$, a minimum located around $x \approx 7.3 \times 10^{-3}$ with η value about -73 is not shown.

cases are numerically well behaved, P1 is not a good choice in that further refinement with larger m quickly leads to large, problematic variations of $\eta(x)$ and poor accuracy of the calculated free energy F_s. We attribute the deep cusp at $x=\tau$ to the fact that ϕ_0' is discontinuous at this point; as indicated in Fig. 2(a), using larger m results in deeper cusp and wild oscillations of $\eta(x)$ around $x=\tau$. From Eq. (4) one

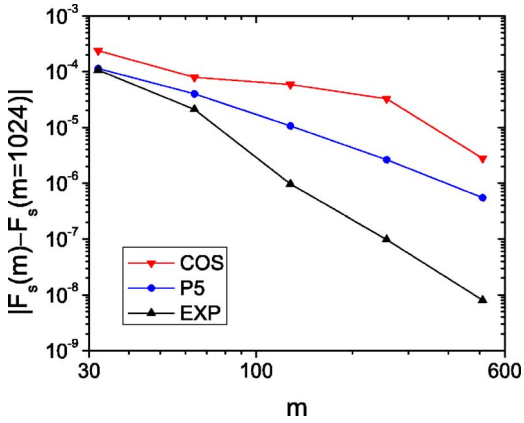

FIG. 3. Influence of spatial-domain discretization on the accuracy of free-energy calculations for confined homopolymers. $d \approx 3.7237$ and $n=2048$. The τ values are given in the caption of Fig. 2. Here we approximate the exact value of F_s (obtained when $m \to \infty$) by that calculated with the largest m, $F_s(m=1024)$.

can also see that $\eta^{\mathrm{GSDA}}(x)$ for P1 is discontinuous at $x=\tau$. Moreover, using $\eta^{\mathrm{GSDA}}(x)$ for P1 in Eq. (3) results in a diverging free energy F_s.

That $\eta(x)$ seems to follow $\eta^{\mathrm{GSDA}}(x)$ in Fig. 1 leads to the following idea of reducing the variations of $\eta(x)$ in the surface layer: By setting $\eta^{\mathrm{GSDA}}(x)=0$ in Eq. (4) and using the boundary conditions of $\phi_{0,\mathrm{sl}}(x=0)=0$ and $\phi_{0,\mathrm{sl}}(x=\tau)=1$, we obtain a quadratic profile of $\phi_{0,\mathrm{sl}}(x)=(x/\tau)^2$ (referred to as P2). The numerically solved $\eta(x)$ for P2 is shown in Fig. 2(a), where $d \approx 3.7237$ and $\tau=0.3$ are used, to be consistent with the calculations below. Similar to the P1 case, the discontinuity of ϕ_0' at $x=\tau$ unfortunately leads to a deep cusp and wild oscillations of $\eta(x)$ around this point, thus poor accuracy of the calculated F_s. This is probably also responsible for the deviation of $\eta(x)$ from $\eta^{\mathrm{GSDA}}(x)$ in the surface layer. The oscillations of $\eta(x)$ very close to the surface can be alleviated by using larger n (data not shown).

Matsen used a cosine profile of $\phi_{0,\mathrm{sl}}(x)=[1-\cos(\pi x/\tau)]/2$ (referred to as COS),[21] which eliminates the discontinuity of ϕ_0' at $x=\tau$. Figure 2(a) also shows the obtained $\eta(x)$ for this profile. We see that COS is better than both P1 and P2 in that the variation of $\eta(x)$ is much smaller. However, $\eta^{\mathrm{GSDA}}(x)$ is discontinuous at $x=\tau$, which is probably responsible for the deviation of $\eta(x)$ from $\eta^{\mathrm{GSDA}}(x)$ in the surface layer. Nevertheless, COS allows converging free-energy calculations, as shown in Fig. 3. Our results also indicate that, as in the P2 case, the oscillations of $\eta(x)$ very close to the surface can be alleviated by using larger n (data not shown).

From these results, it seems critical that both ϕ_0' and $\eta^{\mathrm{GSDA}}(x)$ need to be continuous at $x=\tau$ in order to further improve the numerical performance of SCF calculations. Requiring $\phi_{0,\mathrm{sl}}(x=0)=\phi_{0,\mathrm{sl}}'(x=0)=0$, $\phi_{0,\mathrm{sl}}(x=\tau)=1$, and $\phi_{0,\mathrm{sl}}'(x=\tau)=\phi_{0,\mathrm{sl}}''(x=\tau)=\phi_{0,\mathrm{sl}}'''(x=\tau)=0$ (the last condition ensures the continuity of η' at $x=\tau$), we obtain a fifth-order polynomial of $\phi_{0,\mathrm{sl}}(x)=-4(x/\tau)^5+15(x/\tau)^4-20(x/\tau)^3+10(x/\tau)^2$ (referred to as P5). Figure 2(b) shows the numerically solved $\eta(x)$ for this profile; we see that smoothly varying $\eta(x)$, which closely follows $\eta^{\mathrm{GSDA}}(x)$, can be obtained by using large enough n. The free-energy calculation using P5 also

has higher accuracy than using COS, as shown in Fig. 3; in particular, the error of F_s calculated using P5 decays nicely with $m^{-1.9}$.

Finally, we note that for confined homopolymer *solutions* $\nabla^2 q$ is 0 for all s at the surfaces. Although we prefer not to introduce a small-molecule solvent into the system due to the complication of additional interaction parameters between the solvent and polymers, this property can be utilized to construct $\phi_0(x)$ that eliminates the divergence of $\eta^{\mathrm{GSDA}}(x)$ at $x=0$. After some trials, we find that $\phi_{0,\mathrm{sl}}(x) = \{\exp[4\tau x/(\tau^2-x^2)]-1\}^2/\{\exp[4\tau x/(\tau^2-x^2)]+1\}^2$ (referred to as EXP) gives so far the best numerical performance. Although this profile looks very close to COS when plotted, Fig. 3 shows that the error of F_s calculated using EXP decays with $m^{-3.4}$ for $m \geqslant 128$, much better than that using COS. Figure 2(c) shows the obtained $\eta(x)$ for this profile, where we see some oscillations of $\eta(x)$ very close to the surface (which can be alleviated by using larger n). We also see some deviation of $\eta(x)$ from $\eta^{\mathrm{GSDA}}(x)$ very close to the surface. Both of these, however, do not affect its superior numerical performance.

B. Segmental distributions

It is well known that polymer chains close to an impenetrable (hard) surface lose entropy, and that chain ends lose less entropy than middle segments when close to the surface. We therefore expect the enrichment of chain ends and depletion of middle segments near a hard surface. To quantify this, we define the reduced distribution function of the (sN)th segment as

$$\rho(x,s) = \frac{\bar{\phi}_0 q(x,s) q(x,1-s)}{Q\phi_0(x)}, \tag{13}$$

such that a constant $\rho(x,s)$ indicates a uniform distribution of the segment.

Figure 4 shows the end-segment and the middle-segment distributions, $\rho(x,s=0)$ and $\rho(x,s=0.5)$, respectively, for homopolymer melts confined by either EXP ($\tau \approx 0.5303$) or P5 profile ($\tau=0.6$) with $d \approx 3.7237$; the corresponding results of using COS profile ($\tau=0.4$) are hardly distinguishable from those of using EXP, thus not shown. In all cases, we see that chain ends are enriched near hard surfaces and that $\rho(x,s=0)$ is inversely proportional to the distance to a surface as the surface is approached. This can be understood by invoking the GSDA, which leads to $\rho(x,s) \propto \phi_0^{-1/2}(x)$ for $s=0$ or 1; note that $\phi_{0,\mathrm{sl}}(x) \sim O(x^2)$ as $x \to 0$ for EXP, P5 and COS profiles. On the other hand, the middle segments are depleted from hard surfaces, and GSDA gives $\rho(x,s) \sim O(1)$ for $0 < s < 1$. Comparing Fig. 4(a) with Fig. 4(b), we see that the range of middle-segment depletion is larger than that of chain-end enrichment.

Although we study in this section the simplest system of confined homopolymer melts, the above hard-surface effects are generic for all confined polymeric systems. For example, the influence of $\phi_0(x)$ on ω fields near the surfaces in the case of confined diblock copolymers A-B is the same as that in the homopolymer case (data not shown). The chain-end enrichment and middle-segment depletion in the diblock copolymer case, however, are further complicated by A-B repulsion (thus microphase separation between A and B) and copolymer composition f_A, as revealed below.

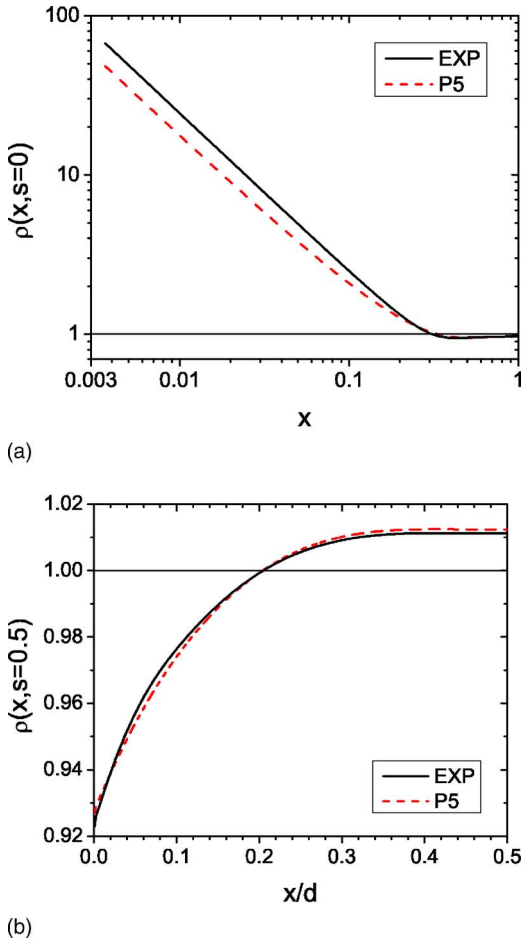

FIG. 4. Reduced distributions of (a) the end segments and (b) the middle segments in confined homopolymer melts, where $d \approx 3.7237$, $m=1024$, and $n=8192$. The τ values are given in the caption of Fig. 2. The results of using COS profile are hardly distinguishable from those of using EXP, thus not shown. In the log-log plot shown in part (a), the curves approach a slope of -1 as $x \to 0$. In part (b), the curves are symmetric about $x=d/2$. Under the bulk condition ($\phi_0(x)=1$) a constant value of 1 is expected for these distributions.

IV. CONFINED SYMMETRIC DIBLOCK COPOLYMER MELTS

A. Surface-induced compatabilization

For confined diblock copolymer melts, the decrease of $\phi_{0,\mathrm{sl}}(x)$ from 1 reduces the A-B repulsion in the surface layer; this is referred to as the "surface-induced A-B compatibilization" or "negative line tension."[21] This energetic effect therefore favors the morphology where more A-B interfaces (which contribute the most to the A-B repulsion) can present in the surface layer. In the case of symmetric diblock copolymers, this has been considered as the dominant factor responsible for the interesting phenomenon that, when the film thickness d is commensurate with the bulk lamellar period l_0, perpendicular lamellae are more stable than parallel lamellae in thin films confined between two neutral surfaces.[21,24,28]

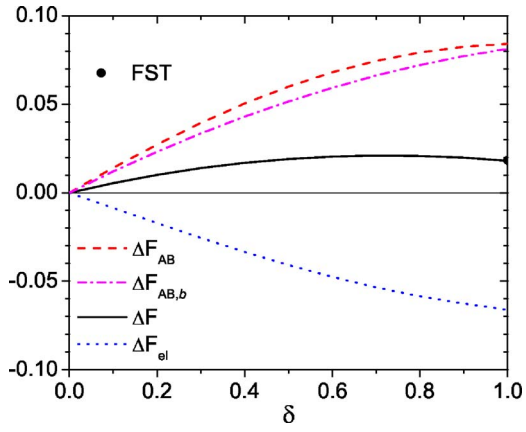

FIG. 5. Free-energy differences between parallel and perpendicular lamellae of symmetric diblock copolymers ($f_A=0.5$ and $\chi N=15$) between two neutral surfaces separated at $d=l_0\approx 3.7137$. Here we use $\phi_{0,\mathrm{sl}}(x)=1-[1+\cos(\pi x/\tau)]\delta/2$ (with $\tau=0.2$) such that adjusting δ from 0 to 1 changes $\phi_{0,\mathrm{sl}}(x)$ from 1 to COS profile, and accordingly the Neumann boundary conditions in the x direction. The dot at $\delta=1$ represents ΔF calculated using the Dirichlet boundary conditions, where the fast sine transforms are used accordingly.

By defining the reduced A-segmental density $\tilde{\phi}_A(\mathbf{r})\equiv\phi_A(\mathbf{r})/\phi_0(x)$, the A-B interaction energy per chain can be written as

$$F_{AB}\equiv\frac{\chi N}{\bar{\phi}_0 V}\int d\mathbf{r}\phi_A(\mathbf{r})\phi_B(\mathbf{r})$$
$$=\frac{\chi N}{\bar{\phi}_0 V}\int d\mathbf{r}\tilde{\phi}_A(\mathbf{r})[1-\tilde{\phi}_A(\mathbf{r})]\phi_0^2(x), \quad (14)$$

where Eq. (9) is used. To quantify the surface-induced compatibilization, we consider the difference in F_{AB} between the parallel and perpendicular lamellae (denoted by $\parallel$ and $\perp$, respectively), $\Delta F_{AB}\equiv F_{AB}^{\parallel}-F_{AB}^{\perp}$, confined between two neutral surfaces. Here we set $\chi N=15$ and $d=l_0\approx 3.7137$, and use $\phi_{0,\mathrm{sl}}(x)=1-[1+\cos(\pi x/\tau)]\delta/2$ with $\tau=0.2$ in our calculations such that adjusting δ from 0 to 1 changes $\phi_{0,\mathrm{sl}}(x)$ from 1 to COS profile. For both morphologies, if we assume that introducing the hard-surface confinement does not change the *reduced* density, i.e., $\tilde{\phi}_A(\mathbf{r})=\phi_{A,b}(\mathbf{r})$ with $\phi_{A,b}(\mathbf{r})$ being the density profile under the bulk condition of $\phi_0(x)=1$, ΔF_{AB} can then be approximated by

$$\Delta F_{AB,b}=\frac{\chi N}{\bar{\phi}_0 V}\int d\mathbf{r}\{\phi_{A,b}^{\parallel}(\mathbf{r})[1-\phi_{A,b}^{\parallel}(\mathbf{r})]$$
$$-\phi_{A,b}^{\perp}(\mathbf{r})[1-\phi_{A,b}^{\perp}(\mathbf{r})]\}\phi_0^2(x), \quad (15)$$

which can be calculated from the bulk structure and $\phi_0(x)$.

Figure 5 shows that, under the bulk condition ($\delta=0$), lamellae of different orientations degenerate. As δ increases from 0, ΔF_{AB} monotonically increases, indicating that the surface-induced compatibilization favors perpendicular lamellae over parallel ones. The difference between ΔF_{AB} and $\Delta F_{AB,b}$, although small, suggests the change of chain conformations from the bulk counterparts. This is clearly indicated by the large difference between ΔF_{AB} and $\Delta F\equiv F^{\parallel}-F^{\perp}$; the latter even exhibits a maximum at $\delta\approx 0.7$. This leads to the entropic effects of hard-surface confinement, which have been overlooked in previous studies.[21,24,28]

B. Surface-induced entropy loss

The entropic contribution of the copolymer chains to the system free energy is given by

$$F_{\mathrm{el}}\equiv-\frac{1}{\bar{\phi}_0 V}\int d\mathbf{r}[\omega_A(\mathbf{r})\phi_A(\mathbf{r})+\omega_B(\mathbf{r})\phi_B(\mathbf{r})]-\ln Q. \quad (16)$$

As shown in Fig. 5, $\Delta F_{\mathrm{el}}\equiv F_{\mathrm{el}}^{\parallel}-F_{\mathrm{el}}^{\perp}$ monotonically decreases with increasing δ, indicating that the entropic effects actually favor parallel lamellae over perpendicular ones. Figure 5 further indicates that both the energetic and entropic effects have about the same magnitude, and that the competition between them gives rise to the maximum of ΔF.

The reduced distribution function of the (sN)th segment on a copolymer chain is given by

$$\rho(\mathbf{r},s)=\frac{\bar{\phi}_0 q(\mathbf{r},s)q^{*}(\mathbf{r},1-s)}{Q\phi_0(x)}. \quad (17)$$

Again, a constant $\rho(\mathbf{r},s)$ indicates a uniform distribution of the segment. Figure 6 shows the reduced distributions of A ends and A-B joints, $\rho(x,s=0)$ and $\rho(x,s=0.5)$, respectively, in parallel lamellae of 1.5 periods confined between two neutral surfaces separated at $d=1.5l_0$, where we compare the case of hard-surface confinement (EXP profile with $\tau=0.4$) with that under the bulk condition [$\phi_0(x)=1$]. We clearly see in Fig. 6(a) the chain-end enrichment near both surfaces (the B-end distribution can be obtained by the symmetry between A and B), as well as the effects of microphase separation between A and B on the chain-end enrichment. The hard-surface effects on the joint-segment distribution, as shown in Fig. 6(b), are more interesting: While A-B joints are "squeezed" towards the interior of the film as expected, $\rho(x,s=0.5)$ exhibits small increase in the vicinity of the surfaces in comparison to the minima in the interior of the film (i.e., at $x/d\approx 0.35$). Such increase, although entropically unfavorable, is due to the surface-induced A-B compatibilization favoring more A-B joints near the surfaces.

Figure 7 shows $\rho(x,s=0)$ and $\rho(x,s=0.5)$ in perpendicular lamellae (microphase separated along the y direction) confined between two neutral surfaces separated at $d=1.5l_0$, where we again compare the case of hard-surface confinement (EXP profile with $\tau=0.4$) with that under the bulk condition [$\phi_0(x)=1$]. To highlight the influence of microphase separation, two y values are chosen: For A-end distribution shown in Fig. 7(a), we choose the center of A-rich domains [where $\phi_A(y)$ reaches a maximum value of 0.9403] and that of B-rich domains [where $\phi_A(y)$ reaches a minimum value of 0.0597]; for A-B joints shown in Fig. 7(b), we choose the center of either A- or B-rich domains and the A-B interface [where $\phi_A(y)=\phi_B(y)$]. As in the parallel lamellae case, in Fig. 7(a) we clearly see the chain-end enrichment near hard surfaces and the effects of microphase separation on the enrichment. In Fig. 7(b), we see the depletion of joint segments

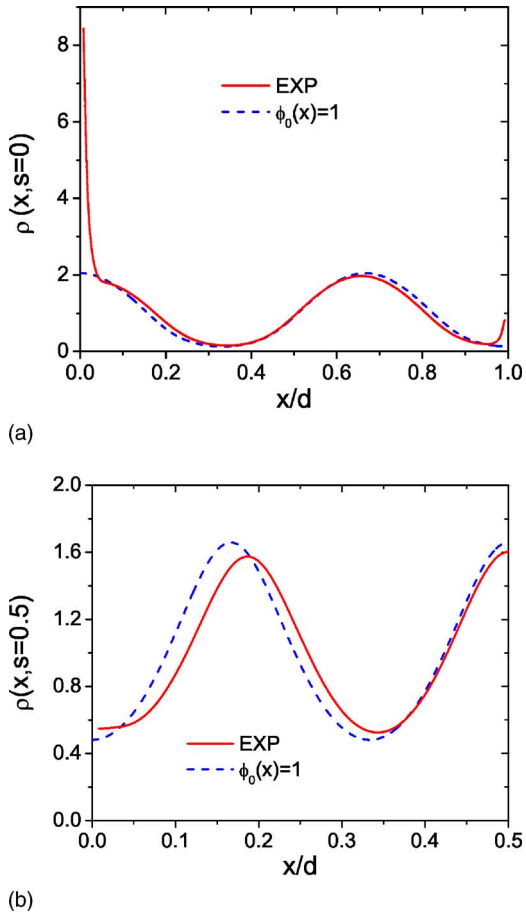

FIG. 6. Reduced distributions of (a) A ends and (b) A-B joints in parallel lamellae of symmetric diblock copolymers ($f_A=0.5$ and $\chi N=15$) of 1.5 periods confined between two neutral surfaces separated at $d=1.5l_0\approx 5.5706$. Here we compare the case of hard-surface confinement (EXP profile with $\tau=0.4$) with that under the bulk condition ($\phi_0(x)=1$). The B-end distribution can be obtained by the symmetry between A and B.

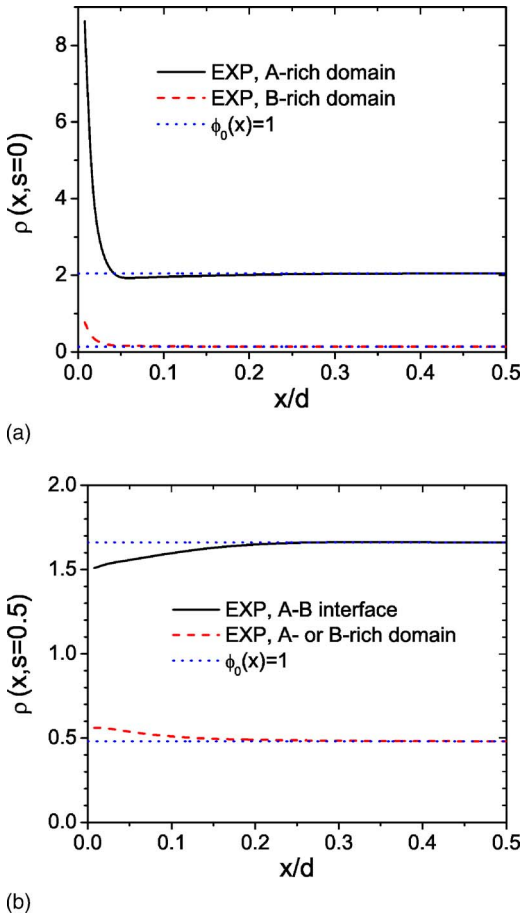

FIG. 7. Reduced distributions of (a) A ends and (b) A-B joints in perpendicular lamellae of symmetric diblock copolymers ($f_A=0.5$ and $\chi N=15$, microphase separated along the y direction) confined between two neutral surfaces separated at $d=1.5l_0\approx 5.5706$. Here we compare the case of hard-surface confinement (EXP profile with $\tau=0.4$) with that under the bulk condition ($\phi_0(x)=1$). The B-end distribution can be obtained by the symmetry between A and B. In the legend, the A-rich domain corresponds to a y value where $\phi_A(y)$ reaches a maximum of 0.9403, the B-rich domain corresponds to a y value where $\phi_A(y)$ reaches a minimum of 0.0597, and the A-B interface is where $\phi_A(y)=\phi_B(y)$.

from the surfaces when their density is high (e.g., at A-B interfaces), while the surface-induced A-B compatibilization causes some increase of joint segments in the vicinity of the surfaces when their density is low (e.g., at the center of A- or B-rich domains). Comparing Figs. 6 and 7, we see that, overall, there are more chain ends and less joint segments near surfaces in parallel lamellae than in perpendicular lamellae; the entropic effects therefore favor parallel lamellae, consistent with ΔF_{el} shown in Fig. 5. We note that the chain-end effect on lamellar orientation was analyzed by Pickett and co-workers.[39,40]

C. Influence of $\phi_0(x)$ on phase behavior

To quantify the influence of various functional forms of $\phi_0(x)$ and the τ values on the phase behavior of confined diblock copolymers, we consider symmetric diblock copolymers ($\chi N=15$) confined between two identical surfaces preferring A block separated at $d=l_0$. Here we use a surface field symmetric about $x=d/2$, $H(x)=\Lambda[1+\cos(\pi x/\tau)]/2$ in the surface layer and 0 elsewhere (with $\Lambda>0$ denoting the strength of surface preference), and focus on how the value of Λ at the phase boundary between parallel lamellae of one period and perpendicular lamellae, Λ_0, changes with different choices of $\phi_{0,\mathrm{sl}}(x)$ and τ.

We obtain $\Lambda_0\approx 1.89$ for EXP profile with $\tau=0.4$, and $\Lambda_0\approx 2.06$ for COS profile with $\tau\approx 0.3017$ (which gives the same $\bar{\phi}_0$ as the EXP profile). The functional forms of $\phi_0(x)$ therefore only have minor influence on the phase behavior, and hence can be chosen based on the numerical performance of SCF calculations. On the other hand, using EXP profile with $\tau=0.2$ changes Λ_0 to 0.64; the influence of τ is therefore more significant, as expected.

Although depending on the functional form of $H(x)$, these Λ_0 values can be compared with that of χN, indicating that the hard-surface effects are weak in practice. Therefore, although these effects exist in all confined polymeric systems, they are manifested only when the surfaces are nearly neutral. This supports the idea of ignoring hard-surface effects for stronger surface preference, where one can use the bulk condition of $\phi_0(x)=1$ (thus the Neumann boundary conditions) for confined systems to avoid large m values needed to resolve the surface layer.

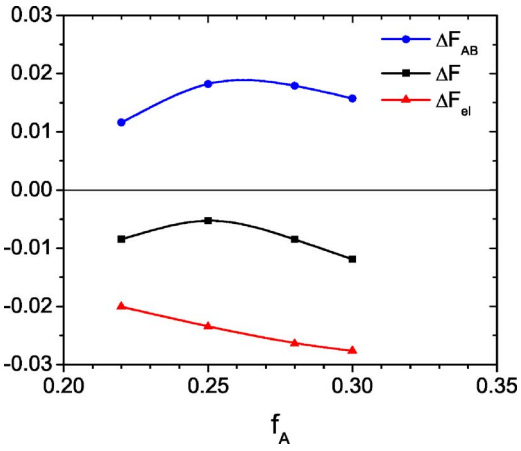

FIG. 8. Free-energy differences between parallel and perpendicular cylinders of asymmetric diblock copolymers ($\chi N=25$) confined by EXP profile ($\tau=0.4$) between two neutral surfaces separated at $d=\sqrt{3}l_0$. $l_0\approx 3.9266$, 4.1266, 4.2832, and 4.4068 for $f_A=0.22$, 0.25, 0.28, and 0.3, respectively. The data points are actual calculations, and the curves are guide to the eyes only. $l_y=l_0$ and $l_z=\sqrt{3}l_0$ (for perpendicular cylinders) are used in our calculations.

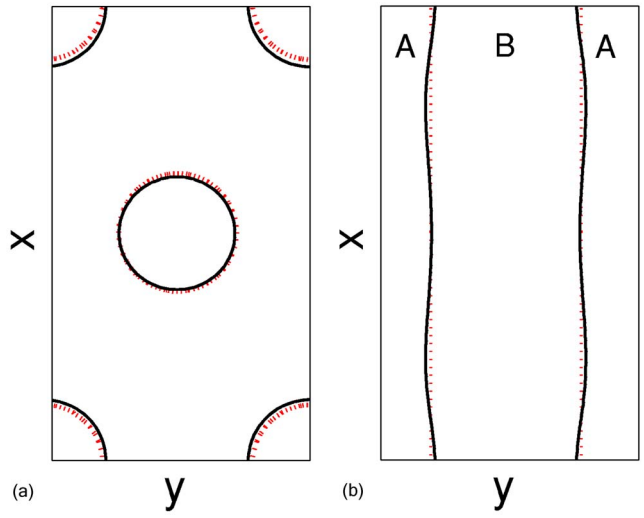

FIG. 9. *A-B* interfaces [where $\phi_A(\mathbf{r})=\phi_B(\mathbf{r})$] in (a) parallel cylinders (whose axis is along the z direction) and (b) perpendicular cylinders of asymmetric diblock copolymers ($f_A=0.22$ and $\chi N=25$) confined between two neutral surfaces separated at $d=\sqrt{3}l_0\approx 6.8010$. The solid curves show the results under confinement by EXP profile ($\tau=0.4$), and the dotted curves show corresponding results under the bulk condition ($\phi_0(x)=1$). $l_y=l_0$ and $l_z=\sqrt{3}l_0$ (for perpendicular cylinders) are used in our calculations.

V. CONFINED ASYMMETRIC DIBLOCK COPOLYMERS

For symmetric diblock copolymers confined between two identical surfaces, the hard surfaces affect the two blocks equally due to the symmetry between them. This is not the case for confined asymmetric diblock copolymers. Both dynamic density-functional calculations[41] and lattice Monte Carlo simulations[31] have revealed an entropic preference of a hard surface for the shorter block. We therefore investigate the hard-surface effects on cylinder-forming asymmetric diblock copolymers in this section.

A. Hard-surface effects

Figure 8 shows the free-energy difference between parallel and perpendicular cylinders, as well as its energetic and entropic components, for cylinder-forming asymmetric diblock copolymers ($\chi N=25$) confined by EXP profile ($\tau=0.4$) between two neutral surfaces separated at $d=\sqrt{3}l_0$, where l_0 here represents the smallest intercylinder distance in the bulk. Interestingly, we see that the surface-induced entropy loss favoring parallel cylinders now outweighs the surface-induced *A-B* compatibilization favoring perpendicular cylinders. Without further calculations, however, one should not generalize this result to other values of χN and f_A.

For the case of $f_A=0.22$, Fig. 9 shows in solid curves the *A-B* interfaces [where $\phi_A(\mathbf{r})=\phi_B(\mathbf{r})$] in these two morphologies; corresponding results under the bulk condition [$\phi_0(x)=1$] are also shown in dots. We see enlargement of *A*-rich regions near the hard surfaces, which results in the shrinkage of *A* cylinders in the interior of the film in the case of parallel cylinders and the undulation of *A-B* interfaces in the case of perpendicular cylinders. The neutral, hard surfaces indeed exhibit preference for the shorter (*A*) block.

To examine the change in chain conformations due to the hard-surface confinement, Fig. 10 shows the reduced distributions of *A* ends, *B* ends, and *A-B* joints in these two morphologies. As in the case of confined symmetric diblock copolymers, we clearly see chain-end enrichment near hard surfaces and the effects of microphase separation between *A* and *B* on the enrichment. For parallel cylinders, Fig. 10(c) further shows the depletion of joint segments from the surfaces when their density is high (e.g., at *A-B* interfaces), while the surface-induced *A-B* compatibilization causes small increase of joint segments in the vicinity of the surfaces when their density is low (e.g., at the center of *B*-rich domains). For perpendicular cylinders, we note that the overall enrichment of joint segments near hard surfaces is caused not only by the surface-induced *A-B* compatibilization, but also by the entropic preference of the surfaces for the shorter block. Overall (data not shown), there are more chain ends near surfaces in parallel cylinders than in perpendicular cylinders; the entropic effects therefore favor parallel cylinders, consistent with ΔF_{el} shown in Fig. 8. Comparing *A* with *B* ends, however, we see that the chain-end enrichment is more pronounced for the shorter (*A*) block. This is the case not only for cylinder-forming asymmetric diblock copolymers as shown in Fig. 10, but also for lamellae-forming asymmetric diblock copolymers (e.g., $f_A=0.4$ and $\chi N=15$; data not shown). This phenomenon is caused by *A-B* repulsion ($\chi>0$), since for confined homopolymers (effectively $\chi=0$) both chain ends enrich equally. The entropic preference of a hard surface for the shorter block was explained in Ref. 31 based on chain-end enrichment and chain connectivity (i.e., the shorter block is on average closer to a chain end than the longer block); it occurs even for equal enrichment of *A* and *B* ends. *A-B* repulsion therefore enhances this entropic preference.

B. Effectively neutral surface

The undulation of *A-B* interfaces in perpendicular cylinders shown in Fig. 9(b) is a manifestation of the entropic

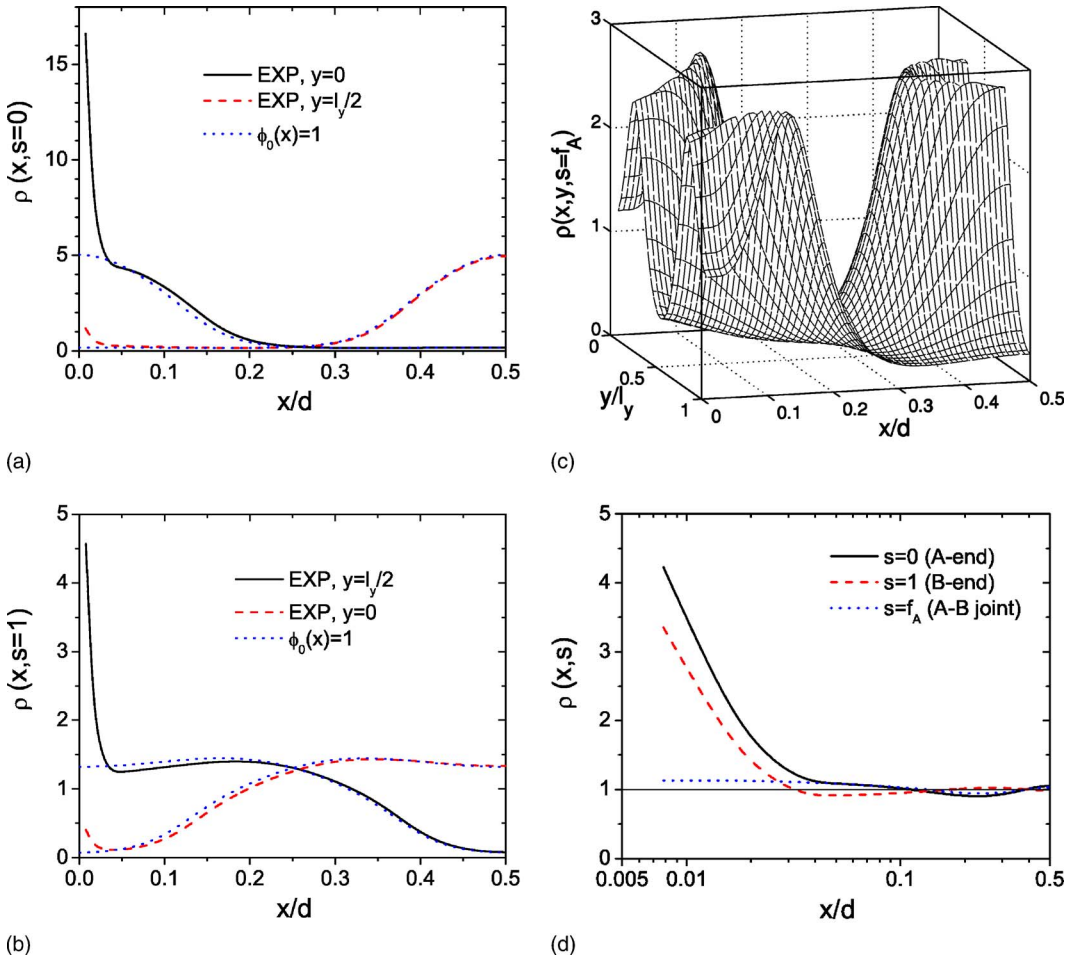

FIG. 10. Reduced distributions of (a) *A* ends, (b) *B* ends, and (c) *A*-*B* joints in parallel cylinders of asymmetric diblock copolymers ($f_A=0.22$ and $\chi N=25$) confined between two neutral surfaces separated at $d=\sqrt{3}l_0\approx 6.8010$. In parts (a) and (b) we compare the case of hard-surface confinement (EXP profile with $\tau=0.4$) with that under the bulk condition ($\phi_0(x)=1$), and use two y values corresponding to Fig. 9(a). In part (c) only the results of hard-surface confinement are shown for clarity. Part (d) shows these distributions in perpendicular cylinders, where $\rho(x,s)$ represents the average over y and z directions, and under the bulk condition a constant value of 1 is expected for these distributions. In all cases, the distributions are symmetric about $x=d/2$, and $l_y=l_0$ and $l_z=\sqrt{3}l_0$ (for perpendicular cylinders) are used in our calculations.

preference of hard surfaces for the shorter block. To quantify this entropic preference, we introduce an energetic preference of the surfaces for the longer (B) block, i.e., $\Lambda<0$, and characterize the undulation by

$$A_u \equiv \frac{1}{l_y l_z}\int \mathrm{d}y\mathrm{d}z \frac{\phi_A(x=d/m,y,z)}{\phi_0(x=d/m)} - f_A. \tag{18}$$

At $\Lambda=\Lambda_0$, A_u vanishes and we have effectively neutral surfaces, near which both chain ends are equally enriched (data not shown).

For perpendicular cylinders ($\chi N=25$) confined by EXP profile ($\tau=0.4$) between two identical surfaces separated at $d=\sqrt{3}l_0$, we obtain $\Lambda_0\approx -2.72$ and -1.51 for $f_A=0.22$ and 0.3, respectively. As expected, the entropic preference is stronger for more asymmetric diblock copolymers. Similar to the hard-surface effects for confined symmetric diblock copolymers, however, such entropic preference is weak in practice.

VI. CONCLUSIONS

We have investigated several effects due to the confinement of polymer melts by impenetrable (hard) surfaces in the self-consistent field (SCF) calculations. To adequately represent such confinement, the total (normalized) polymer segmental density is usually constrained to an imposed profile $[\phi_0(x)]$ that continuously decreases from 1 in the interior of confined melts (bulk condition) to 0 at the surfaces over a short distance (surface layer). The choice of this profile in the surface layer, $\phi_{0,\mathrm{sl}}(x)$, strongly influences the numerical performance of the self-consistent field calculations. We have identified two profiles (P5 and EXP) of $\phi_{0,\mathrm{sl}}(x)$, which make the calculations converge rapidly with refined discretization.

Hard-surface confinement also changes chain conformations from the bulk counterparts, leading to the enrichment of chain ends and depletion of middle segments near the surfaces. For confined diblock copolymers *A*-*B*, these entropic effects favor parallel morphologies where chains orient mainly perpendicular to the surfaces. They are, however, further complicated by *A*-*B* repulsion (thus microphase sepa-

ration between A and B) and copolymer composition f_A. The decrease of polymer density from 1 reduces A-B repulsion and favors morphologies with more A-B interfaces near the surfaces. Such surface-induced A-B compatibilization (energetic effect) therefore acts against the depletion of A-B joints from the surfaces. In the case of symmetric diblock copolymers confined between two neutral surfaces, when the film thickness is commensurate with the bulk lamellar period, the energetic effect favoring perpendicular lamellae outweighs the entropic effects. The latter, however, are comparable in magnitude to the former and cannot be overlooked. For confined asymmetric diblock copolymers, the chain-end enrichment results in an entropic preference of a neutral surface for the shorter block, which is enhanced by A-B repulsion.[31]

Our calculations also show that different functional forms of $\phi_{0,\mathrm{sl}}(x)$ only have minor influence on the phase behavior of confined diblock copolymers, and hence can be chosen based on the numerical performance of SCF calculations. After all, the hard-surface effects are weak in practice and thus manifested only when the surfaces are nearly neutral. This supports the idea of ignoring hard-surface effects for stronger surface preference, where one can use the bulk condition of $\phi_0(x)=1$ (thus the Neumann boundary conditions) for confined systems to avoid the large number of collocation points needed to resolve the surface layer.

ACKNOWLEDGMENTS

Q.W. thanks Professor Glenn Fredrickson, Professor Carlos Garcia-Cervera, and Professor Eric Cochran for helpful discussions on the fourth-order implicit-explicit scheme. Financial support for this work was provided by Colorado State University, which is gratefully acknowledged.

[1] S. F. Edwards, Proc. Phys. Soc. London **85**, 613 (1965).
[2] E. Helfand and Y. Tagami, J. Polym. Sci., Part B: Polym. Lett. **9**, 741 (1971).
[3] E. Helfand and Y. Tagami, J. Chem. Phys. **56**, 3592 (1972); **57**, 1812 (1972).
[4] E. Helfand and A. M. Sapse, J. Chem. Phys. **62**, 1327 (1975).
[5] K. M. Hong and J. Noolandi, Macromolecules **14**, 736 (1981).
[6] J. Noolandi and K. M. Hong, Macromolecules **15**, 482 (1982).
[7] J. Noolandi and K. M. Hong, Macromolecules **17**, 1531 (1984).
[8] K. R. Shull and E. J. Kramer, Macromolecules **23**, 4769 (1990).
[9] K. R. Shull, Macromolecules **26**, 2346 (1993).
[10] M. D. Whitmore and J. D. Vavasour, Acta Polym. **46**, 341 (1995).
[11] M. W. Matsen and F. S. Bates, Macromolecules **29**, 1091 (1996).
[12] M. W. Matsen, J. Phys.: Condens. Matter **14**, R21 (2002).
[13] G. J. Fleer, M. A. Cohen Stuart, J. M. H. M. Scheutjens, T. Cosgrove, and B. Vincent, *Polymers at Interfaces* (Chapman & Hall, London, 1993).
[14] G. J. Fleer and F. A. M. Leermakers, Curr. Opin. Colloid Interface Sci. **2**, 308 (1997).
[15] M. W. Matsen and M. Schick, Phys. Rev. Lett. **72**, 2660 (1994).
[16] G. Tzeremes, K. O. Rasmussen, T. Lookman, and A. Saxena, Phys. Rev. E **65**, 041806 (2002).
[17] E. W. Cochran, C. J. Garcia-Cervera, and G. H. Fredrickson, Macromolecules **39**, 2449 (2006); **39**, 4264 (2006).
[18] H. D. Ceniceros and G. H. Fredrickson, Multiscale Model. Simul. **2**, 452 (2004).
[19] S. W. Sides and G. H. Fredrickson, Polymer **44**, 5859 (2003).
[20] E. Helfand and Z. R. Wasserman, Macromolecules **11**, 960 (1978).
[21] M. W. Matsen, J. Chem. Phys. **106**, 7781 (1997).
[22] H. Y. Chen and G. H. Fredrickson, J. Chem. Phys. **116**, 1137 (2002).
[23] W. H. Li, R. A. Wickham, and R. A. Garbary, Macromolecules **39**, 806 (2006).
[24] T. Geisinger, M. Muller, and K. Binder, J. Chem. Phys. **111**, 5241 (1999).
[25] I. W. Hamley, Nanotechnology **14**, R39 (2003).
[26] M. Lazzari and M. A. Lopez-Quintela, Adv. Mater. (Weinheim, Ger.) **15**, 1583 (2003).
[27] C. Park, J. Yoon, and E. L. Thomas, Polymer **44**, 6725 (2003).
[28] W. H. Tang, Macromolecules **33**, 1370 (2000).
[29] J. U. Sommer, A. Hoffmann, and A. Blumen, J. Chem. Phys. **111**, 3728 (1999).
[30] Q. Wang, Q. L. Yan, P. F. Nealey, and J. J. de Pablo, J. Chem. Phys. **112**, 450 (2000).
[31] Q. Wang, P. F. Nealey, and J. J. de Pablo, Macromolecules **34**, 3458 (2001).
[32] G. H. Fredrickson, *The Equilibrium Theory of Inhomogeneous Polymers* (Oxford University Press, Oxford, 2006).
[33] W. H. Press, S. A. Teukolsky, W. T. Vetterling, and B. P. Flannery, *Numerical Recipes in C: The Art of Scientific Computing*, 2nd ed. (Cambridge University Press, Cambridge, 2002), Chap. 16.4.
[34] W. H. Press, S. A. Teukolsky, W. T. Vetterling, and B. P. Flannery, *Numerical Recipes in C: The Art of Scientific Computing*, 2nd ed. (Cambridge University Press, Cambridge, 2002), Chap. 9.7.
[35] W. H. Press, S. A. Teukolsky, W. T. Vetterling, and B. P. Flannery, *Numerical Recipes in C: The Art of Scientific Computing*, 2nd ed. (Cambridge University Press, Cambridge, 2002), Chap. 4.3.
[36] W. H. Li and R. A. Wickham, Macromolecules **39**, 8492 (2006).
[37] K. O. Rasmussen, J. Polym. Sci., Part B: Polym. Phys. **42**, 3695 (2004).
[38] Y. Z. Yang, F. Qiu, H. D. Zhang, and Y. L. Yang, Polymer **47**, 2205 (2006).
[39] G. T. Pickett, T. A. Witten, and S. R. Nagel, Macromolecules **26**, 3194 (1993).
[40] G. T. Pickett and A. C. Balazs, Macromolecules **30**, 3097 (1997).
[41] H. P. Huinink, J. C. M. Brokken-Zijp, M. A. van Dijk, and G. J. A. Sevink, J. Chem. Phys. **112**, 2452 (2000).